Monthly Notices of the ROYAL ASTRONOMICAL SOCIETY

MNRAS **443,** 2252–2263 (2014) doi:10.1093/mnras/stu1349

New detections of HC_5N towards hot cores associated with 6.7 GHz methanol masers

C.-E. Green,[1,2★] J. A. Green,[2,3] M. G. Burton,[1] S. Horiuchi,[4] N. F. H. Tothill,[5] A. J. Walsh,[6] C. R. Purcell,[7] J. E. J. Lovell[8] and T. J. Millar[9]

[1]*School of Physics, University of New South Wales, Sydney, NSW 2052, Australia*
[2]*CSIRO Astronomy & Space Science, Australia Telescope National Facility, PO Box 76, Epping, NSW 2121, Australia*
[3]*SKA Organisation, Jodrell Bank Observatory, Lower Withington, Macclesfield SK11 9DL, UK*
[4]*CSIRO Astronomy & Space Science/NASA, Canberra Deep Space Communication Complex, PO Box 1035, Tuggeranong ACT 2901, Australia*
[5]*University of Western Sydney, Locked Bag 1797, Penrith NSW 2751, Australia*
[6]*International Centre for Radio Astronomy Research, Curtin University, Perth, WA 6845, Australia*
[7]*Sydney Institute for Astronomy, School of Physics, The University of Sydney, NSW 2006, Australia*
[8]*School of Mathematics and Physics, University of Tasmania, Private Bag 37, Hobart 7001, Australia*
[9]*Astrophysics Research Centre, School of Mathematics and Physics, Queens University Belfast, Belfast BT7 1NN, UK*

Accepted 2014 July 3. Received 2014 June 24; in original form 2014 April 16

ABSTRACT

We present new detections of cyanodiacetylene (HC_5N) towards hot molecular cores, observed with the Tidbinbilla 34 m radio telescope (DSS–34). In a sample of 79 hot molecular cores, HC_5N was detected towards 35. These results are counter to the expectation that long chain cyanopolyynes, such as HC_5N, are not typically found in hot molecular cores, unlike their shorter chain counterpart HC_3N. However, it is consistent with recent models which suggest HC_5N may exist for a limited period during the evolution of hot molecular cores.

Key words: astrochemistry – stars: formation – ISM: clouds – ISM: molecules.

1 INTRODUCTION

Molecular clouds support a rich organic chemistry which can be used to ascertain the progress of high-mass star formation within them. High-mass star formation begins when dense ($<10^4$ cm^{-3}) clumps of cold gas and dust inside molecular clouds collapse under their own gravity and form cold (<10 K) cores. This stage proceeds for $\sim5 \times 10^4$ yr. An increase in temperature, caused by the central protostar, and continuing collapse progresses the cloud to the dense ($\sim10^6$ cm^{-3}), hot (>100 K, typically ~200 K) core stage. Ices that were frozen on to dust grains in the previous stage are evaporated, resulting in a time-dependent chemistry in which gas phase reactions produce complex molecules (Chapman et al. 2009). This stage proceeds on a time-scale of $\sim5 \times 10^4$ to $\sim1 \times 10^5$ yr. Methanol (CH_3OH) masers, exclusive markers of high-mass star formation (Minier et al. 2003; Breen et al. 2013) also switch on in this stage (Breen et al. 2010a).

Hot core chemistry is typically dominated by saturated molecules (Olmi, Cesaroni & Walmsley 1993) and methyl cyanide (CH_3CN) is considered a key tracer of the hot core stage (Chapman et al. 2009). Cyanodiacetylene (HC_5N) is an unsaturated, complex organic molecule (a long chain cyanopolyyne, $HC_{2n+1}N$) associated with the early stages of star formation (e.g. Hirota & Yamamoto 2006, Rathborne et al. 2008, Goddi et al. 2009). Although readily detected in cold (10 K), dark (10^4 cm^{-3}) molecular clouds, the detection of HC_5N in warmer gas has proven difficult. Recently, Sakai et al. (2008, 2009) have shown that a warm carbon-chain chemistry (WCCC) occurs in warmer (~20 K), denser ($\sim10^6$ cm^{-3}) gas. In such gas it appears that the increase in grain temperature is sufficient to desorb the most lightly bound molecules, CO, N_2 and CH_4, from grain ices. The subsequent chemical processing of the evaporated CH_4, first to acetylene, C_2H_2, and its derivatives and then to diacetylene, C_4H_2, and larger carbon-chain molecules drives a complex organic chemistry (Aikawa et al. 2008). HC_5N has been detected in two WCCC sources, L1527 and IRAS15398−3359, with column densities a factor of 10–20 smaller than that in TMC–1. Its formation in these sources has not yet been explained as it was not discussed in the papers by Aikawa et al. (2008, 2012). HC_5N is not typically associated with the more evolved hot core stage of high-mass star formation unlike HC_3N (Wyrowski, Schilke & Walmsley 1999). However, rotational transitions of HC_5N have been observed within the Orion Molecular Cloud (Turner 1991) and the Sagittarius B2 (Sgr B2) molecular cloud (Broten et al. 1976; Avery et al. 1979; Turner 1991).

HC_5N was not expected to be detected in hot cores due to the efficiency of hydrogenation on grain surfaces. It is very likely that both HC_5N, and its precursor molecules diacetylene (HC_4H) and its isomer butatrienylidene (H_2CCCC), will undergo addition reactions with hydrogen atoms in the ice mantles that form in cold, dense gas

★E-mail: claire.elise.green@gmail.com

prior to the onset of star formation. Earlier models of hot core chemistry found the formation of the precursors to be inefficient in the hot core and HC_5N abundances were predicted to be small (Millar, Macdonald & Gibb 1997).

More recent chemical modelling, such as by Chapman et al. (2009), using more complex chemical networks for the synthesis of large carbon-chain molecules shows that the precursor molecules can, in fact, be formed efficiently in the hot core stage, driven by the high abundance of acetylene (C_2H_2) in the hot gas and predict that HC_5N can form and exist under the conditions of hot cores. The two major formation routes to HC_5N involve H_2CCCC (Seki et al. 1996) and HC_4H (Fukuzawa, Osamaru & Schaefer 1998) and can be written in combined form as

$$CN + C_4H_2 \rightarrow HC_5N + H. \quad (1)$$

Fukuzawa et al. (1998) showed that the reactions of CN with the higher polyacetylenes to form larger cyanopolyynes were also exothermic and have led to the suggestion that cyanohexatriyne (HC_7N) and cyanooctatetrayne (HC_9N) may also be detectable in hot cores (Chapman et al. 2009).

To test these chemical models of star formation, there is a need to identify chemical species at different evolutionary stages, establishing a chemical clock (e.g. Stahler 1984). For example, Chapman et al. (2009) modelled an evolution of HC_5N to the longer chain cyanopolyynes, HC_7N and HC_9N, suggesting that detection of HC_5N indicates a relatively younger population of sources.

This paper presents new observations of HC_5N towards 79 hot molecular cores. The observations and data reduction are described in Section 2; results including spectra are presented in Section 3; and Section 4 discusses the nature of detections and implications for the chemical evolution of star formation. Conclusions are presented in Section 5.

2 OBSERVATIONS

Observations of 79 hot molecular cores were made with NASA Deep Space Station 34 (DSS–34), a 34 m diameter radio telescope at Tidbinbilla, located near Canberra, Australia. These observations were made in service observing mode across 26 sessions from 2006 July to 2008 May. Observations were spread over the 2006–2008 period due to the nature of the Tidbinbilla telescope availability, which depends on NASA scheduling priorities. Data from one observation block (2008 February 22) were excluded due to poor baselines attributed to bad weather conditions. The $J = 12 \rightarrow 11$ transition of HC_5N was observed at its rest frequency of 31.951 777 GHz towards these 79 sources. Position-switching was used with a typical integration time of ∼1 min per position in an OFF–ON–ON–OFF pattern. Sources were observed with total integration times of on average ∼20 min (for the entire OFF–ON–ON–OFF pattern). The beamwidth was 0.95 arcmin and the pointing accuracy was 2 arcsec. The correlator was configured to give single polarization data with 2048 channels across a 64 MHz bandwidth centred at 31.951 777 GHz. This provides a velocity channel width of 0.29 km s^{-1}. The initial data collected in 2006 were scaled differently than the 2007 and 2008 data due to different observing procedures and set ups. Therefore the 2006 data were used only to verify detections and not to classify a source as a 'detection'. The 2006 data have been excluded from the following discussion and all analyses.

2.1 Source selection

74 of the 79 sources were associated with 6.7 GHz methanol masers and the remaining five were initially considered 'maserless' cores, offset from methanol maser sites by ∼1–18 arcmin. Two of the five 'maserless' cores (G05.89−0.39 and G05.90−0.43) have since been identified as hosting 6.7 GHz methanol masers (Caswell et al. 2010) and the term 'maserless' core will henceforth refer to the remaining three cores, G00.26+0.01, G14.99−0.70 and G15.03−0.71. Sources were selected to correspond to those of Purcell et al. (2006) which represent a subset of the Walsh et al. (1997, 1998, 2003) methanol maser, radio and sub-millimetre surveys. The maserless cores were selected as potential pre-hot core candidates. Two sources, Sgr B2 and G00.26+0.01, were observed as reference sources for the presence of HC_5N across 12 and 8 epochs, respectively. The other 77 sources were observed between one and six times dependent on telescope availability.

2.2 Data reduction

Data reduction was performed using the Australia Telescope National Facility (ATNF) Spectral Analysis Package (ASAP version 4.0.0).[1] One spectrum was produced per source per epoch. Data were not combined across multiple epochs, as is standard, due to the unexpected scaling problems with the 2006 data. Although this was not an issue with the 2007 and 2008 data, the different epochs were reduced separately to ensure any other issues that did arise were isolated. For each spectrum, the reduction process involved taking the quotient of the source and reference scans and implementing a standard gain elevation correction. The antenna gain is empirically modelled by the following polynomial:

$$G(El) = R_0 + R_1 El + R_2(El^2), \quad (2)$$

where El is the elevation (in degrees), G(El) gives the gain-elevation correction,[2] $R_0 = 0.534289 \times 10^{-1}$, $R_1 = 2.9831 \times 10^{-3}$ and $R_2 = -3.16376 \times 10^{-5}$. The scans were aligned in the Local Standard of Rest Kinematic (LSRK) velocity frame and time-weighted averaging was performed according to integration time. A baseline correction and standard Hanning smoothing across eight spectral channels were then applied. Final spectra were converted to the main beam temperature scale (T_{MB}) by scaling by a factor of 0.7 to correct for beam efficiency (Kuiper & Veruttipong, private communication). Gaussian fitting using χ^2 minimization was then applied to the spectra to extract their peak width and centre velocity. The nominal detection limit was three consecutive channels. The average rms for all spectra with detections was 21 mK. Noise levels in spectra of detections and non-detections were similar, with non-detections having an average rms value of 24 mK. A histogram comparing the noise levels of all spectra with detections across multiple epochs and all spectra with non-detections (which includes those for sources classified as having detections for different epochs) is presented in Fig. 1.

We assume the HC_5N emission is optically thin based on the warm temperatures (100–200 K) and likely small beam filling factor (<10 per cent).

[1] http://svn.atnf.csiro.au/trac/asap

[2] http://www.atnf.csiro.au/observers/docs/tid_obs_guide/tid_obs_guide_dss34.html

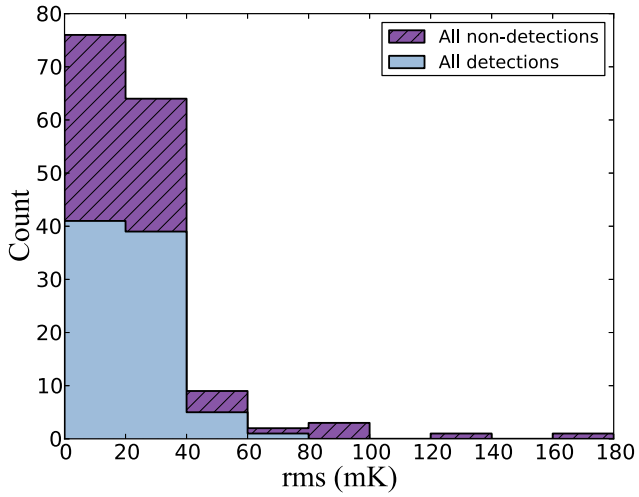

Figure 1. Distribution of rms noise. 'All non-detections' refers to all spectra across multiple epochs with a non-detection of HC_5N. 'All detections' refers to all spectra across multiple epochs with a detection of HC_5N.

3 RESULTS

Cyanodiacetylene (HC_5N) was detected in 35 of the 79 hot molecular cores to a 3σ sensitivity limit of 54 mK. Detections were made at $\sim$3–17σ, where this signal-to-noise ratio was calculated by dividing the unrounded peak T_{MB} by its associated unrounded error (calculated from the rms and Gaussian fit errors). The HC_5N detections included 33 of the maser associated cores and two out of the three 'maserless' cores. The 35 detections include five weak detections at $\lesssim 3\sigma$: G00.55−0.85, G08.14+0.23, G10.48+0.03, G11.50−1.49 and G25.71+0.04. Detections were made for the vast majority of the 35 sources across multiple epochs. The epoch with the best signal-to-noise ratio and weather conditions was then selected. Detections are summarized in Table 1, non-detections are summarized in Table 2 and HC_5N spectra are presented in Fig. 2.

The peak brightness temperature varied between 18 mK (taken to be the 1σ sensitivity limit, giving the 3σ sensitivity limit of 54 mK) and 300 mK (excluding Sgr B2). The majority of sources had HC_5N peak brightness temperatures between 18 and 100 mK. The median peak brightness temperature was 91 mK. The brightest source, excluding Sgr B2, was G05.89−0.39 (300 mK). The distribution of peak brightness temperatures is shown in Fig. 3.

Linewidths (FWHM) varied between 1.0 and 5.1 km s^{-1} (excluding Sgr B2 and G0.26+0.01, both broadened due to their location in the chaotic Galactic Centre). The typical linewidth was 2–3 km s^{-1} and the median was 3.3 km s^{-1}. The source with the widest linewidth, excluding Sgr B2 and G0.26+0.01, was G30.82−0.05 which had a linewidth of 5.1 km s^{-1}. The distribution of the linewidths is shown in Fig. 4.

4 DISCUSSION

4.1 Comparison with methanol maser attributes

Properties of the HC_5N detections and non-detections were compared with the properties of the methanol masers with which they are associated. Fig. 5 compares the distance to the methanol masers with the normalized number of detections and non-detections. As there are unequal numbers of detections and non-detections, normalization sets the total number of detections and non-detections in each bin to unity for ease of comparison. We detect HC_5N across a range of distances and do not see evidence for a fall-off with distance. The majority (6 of the 8 distance bins) have no difference between detections and non-detections with (heliocentric) kinematic distance. This implies either the sample is too small (with results dominated by the statistical errors) or that the sensitivity of these observations is sufficient to detect sources to a distance of $\sim$18 kpc. Fig. 6 compares the peak flux density of the methanol masers with the normalized number of detections and non-detections. Source Sgr B2 has been excluded from this figure as it represents a reference source for the presence of HC_5N and was used as a check of the observations. As one of the largest molecular clouds in the Galaxy, it does not offer good comparison to the rest of the sample and has thus been excluded from all such analyses. Five other sources G00.26+0.01, G00.55−0.85, G14.99−0.70, G15.03−0.71 and G19.47+0.17 were also excluded from this figure due to lack of available data. Again, no clear relation was found in the sample, implying methanol peak flux density is not correlated with the absence or presence of HC_5N.[3]

4.2 Comparison with other molecules

The sources with both HC_5N detections and non-detections were compared with the presence of other molecules. If HC_5N was detected, CH_3CN (5–4 and/or 6–5) (Purcell et al. 2006, 2009) was also detected in all but one source (G11.50−1.49). Both molecules are considered tracers of dense molecular clouds, but although the excitation conditions of these molecules are similar in density, they differ in temperature. HC_5N and CH_3CN have similar critical densities[4] of $\sim 10^5$ and $\sim 10^6$ cm^{-3}, respectively, but the longer carbon-chain HC_5N was expected to be destroyed at the higher temperatures that CH_3CN traces.[4] As discussed in Section 1, CH_3CN is a tracer of the hot core stage of high-mass star formation while HC_5N is more usually associated with the colder and earlier stages of star formation, so the detection of HC_5N in 35 hot molecular cores represents a departure from this paradigm. The detection of HC_5N in these hot molecular cores supports the results of the chemical modelling of Chapman et al. (2009). They found that HC_5N could exist under the conditions of a hot molecular core, and suggest that if HC_5N exists in a region then HC_7N and HC_9N may also have the necessary conditions to form. They also suggest that the abundances of both of these molecules increase over time, although these species are not linked directly, as the rapid gas-phase chemistry begins after the destruction of the grain mantle species (Chapman et al. 2009). Thus, the simultaneous detection of HC_5N and CH_3CN is consistent with the Chapman et al. (2009) results. However, in 25 of the 44 HC_5N non-detection sources, CH_3CN was also detected, contrary to preliminary results presented in Chapman et al. (2009) which indicated that either both HC_5N and CH_3CN were detected together, or neither were detected. Our analysis finds that this is not so and that CH_3CN is detected in both HC_5N detection and non-detection sources.

It is possible that HC_5N can only exist for a limited period of time in these hot molecular cores. This may explain why HC_5N was detected in some of the hot molecular cores in the source list,

[3] http://atoa.atnf.csiro.au/

[4] Critical densities have been calculated assuming a typical hot core temperature of 200 K, a collisional partner of H_2 (giving an average velocity (v) of $\sim$1 km s^{-1}), and a typical collisional cross-section (σ) of 10^{-16} cm^2. The reference for the Einstein A coefficients used for this calculation is the CDMS data base [http://www.astro.uni-koeln.de/cgi-bin/cdmssearch, Müller et al. (2001, 2005)].

Table 1. The 35 HC_5N detections. Column 1 is the Source name; Column 2 is the Date of observation (sources were observed across multiple epochs, the date of observation listed is that of the 'best' individual detection determined by signal-to-noise ratio and weather conditions); Column 3 is the Peak brightness temperature (corrected on to the main beam scale with errors calculated from the rms and Gaussian fit error); Column 4 is the LSRK velocity of the peak of the spectra; Column 5 is the Linewidth (FWHM); Column 6 is the Kinematic distance; Column 7 is the Methanol peak flux density; Column 8 indicates presence of OH masers with an 'o' and water masers with a 'w' (all sources are methanol masers except the three maserless cores); Column 9 indicates the molecules detected, with 'c' indicating CH_3CN (Purcell et al. 2006, except for G11.50−1.49), 'a' indicating HC_3N (reference for this molecule and for the CH_3CN molecule of source G11.50−1.49, is MALT90 Survey data available on the Australia Telescope Online Archive (ATOA)[3]), 'b' indicating HCN, 'd' indicating HNC (Purcell et al. 2006, 2009; additional reference is MALT90 data cubes). A † indicates 'maserless' cores (Purcell et al. 2006). References for quoted peak flux densities, distances and masers are: [a]Caswell et al. (2010), [b]Green et al. (2010), [c]Pestallozzi, Minier & Booth (2005), [d]Green et al. (2012), [f]Green & McClure-Griffiths (2011), [g]Reid et al. (2009), [i]Caswell (1998), [j]Breen et al. (2010b), [k]Forster & Caswell (1989), [l]Caswell et al. (2009). A[h] indicates distance is the kinematic distance calculated from the flat rotation curve with rotation velocity $\theta = 246$ km s^{-1} and solar distance $R_\odot = 8.4$ kpc (Reid et al. 2009; McMillan & Binney 2010; Schönrich et al. 2010).

Source name	Date	Peak T_{MB} (mK)	Vel_{LSRK} (km s^{-1})	Linewidth (FWHM) (km s^{-1})	Distance (kpc)	$S_{Peak\ Methanol}$ (Jy)	Masers	Other molecules
Sgr B2	2007-07-19	390 ± 30	62.1 ± 0.3	19.0 ± 0.4	7.8[g]	–	o[j],w[j]	–
G00.26+0.01†	2007-07-16	140 ± 30	37.5 ± 0.5	12.7 ± 0.9	8.4[h]	–		c,a,b,d
		67 ± 20	20.8 ± 1.9	22.4 ± 4.3				
G00.55−0.85	2008-04-09	69 ± 20	17.8 ± 0.4	4.2 ± 0.8	8.4[h]	61.9[a]	o[j],w[j]	c
G05.89−0.39	2008-04-11	300 ± 20	9.0 ± 0.3	3.5 ± 0.3	1.9[f]	0.5[a]	o[j],w[j]	c,a,b,d
G05.90−0.43	2008-05-14	72 ± 10	7.4 ± 0.3	3.3 ± 0.4	1.6[f]	6.2[a]	w[j]	c,a,b,d
G08.14+0.23	2008-04-11	42 ± 20	18.4 ± 0.4	3.4 ± 0.6	3.2[f]	11.4[b]	w[j]	c,b,d
G08.67−0.36	2008-04-11	93 ± 10	35.2 ± 0.3	4.2 ± 0.3	4.4[f]	10.0[b]	o[j],w[j]	c,a,b,d
G08.68−0.37	2008-03-29	90 ± 06	37.6 ± 0.3	3.3 ± 0.3	4.5[f]	102.0[b]	w[j]	c,a,b,d
G09.62+0.20	2008-03-29	30 ± 07	4.2 ± 0.4	5.0 ± 0.6	5.2[f]	5239.9[b]	o[j],w[j]	c,a,b,d
G10.29−0.13	2008-04-09	68 ± 20	14.1 ± 0.3	3.6 ± 0.5	2.1[h]	7.2[b]	w[j]	c,a,b,d
G10.30−0.15	2008-03-29	38 ± 08	13.7 ± 0.3	3.0 ± 0.4	2.1[h]	0.9[b]		c,a,b,d
G10.32−0.16	2008-03-29	33 ± 08	12.0 ± 0.3	1.8 ± 0.4	1.9[h]	90.1[b]	w[j]	c,a,b,d
G10.34−0.14	2008-04-11	84 ± 20	12.2 ± 0.3	2.1 ± 0.4	1.9[h]	15.1[b]	w[j]	c,a,b,d
G10.47+0.03	2007-07-24	91 ± 20	66.8 ± 0.4	4.4 ± 0.5	11.2[f]	28.0[b]	o[j],w[j]	c,a,b,d
G10.48+0.03	2007-07-24	71 ± 20	65.6 ± 0.4	4.6 ± 0.7	11.4[f]	22.5[b]	o[j],w[j]	c,a,b,d
G10.63−0.33a	2007-09-05	140 ± 30	–4.6 ± 0.3	2.7 ± 0.4	5.2[f]	5.0[b]	w[j]	a,b,d
G10.63−0.38b	2007-09-05	110 ± 30	–2.6 ± 0.3	4.0 ± 0.6	17.0[h]	4.2[b]		c,a,b,d
G11.50−1.49	2008-03-29	18 ± 06	10.4 ± 0.3	2.5 ± 0.5	1.6[f]	68.4[b]	w[j]	c,a,b,d
G11.94−0.62	2008-04-09	120 ± 20	37.6 ± 0.3	3.5 ± 0.3	3.7[f]	42.9[b]		c,a,b,d
G12.68−0.18	2007-09-05	190 ± 30	55.4 ± 0.3	2.8 ± 0.4	4.5[h]	351.0[b]	o[j],w[j]	c,a,b,d
G12.89+0.49	2008-04-09	120 ± 20	32.6 ± 0.3	3.3 ± 0.4	2.3[f]	68.9[b]	o[j],w[j]	c,a,b,d
G12.91−0.26	2007-09-06	63 ± 20	36.4 ± 0.3	4.0 ± 0.2	3.5[h]	269.1[b]	o[j],w[j]	c,a,b,d
G14.99−0.70†	2008-03-29	39 ± 09	18.3 ± 0.3	2.3 ± 0.5	2.0[h]	–		c
G16.86−2.16	2008-04-09	130 ± 20	19.0 ± 0.3	2.8 ± 0.4	1.9[h]	28.9[b]		c
G24.79+0.08	2007-07-19	180 ± 30	110.0 ± 0.3	3.0 ± 0.3	9.6[f]	97.0[c]	o[k],w[k]	c
G25.65+1.05	2007-07-19	84 ± 20	42.4 ± 0.3	1.7 ± 0.4	12.5[f]	178.0[c]		c
G25.71+0.04	2007-07-19	69 ± 30	98.3 ± 0.3	1.0 ± 0.4	10.1[f]	364.0[c]		c
G25.83−0.18	2007-07-19	110 ± 20	93.8 ± 0.3	2.9 ± 0.4	5.0[f]	70.0[c]		c
G28.20−0.05	2007-07-11	140 ± 20	96.1 ± 0.3	2.6 ± 0.4	9.8[f]	3.3[c]	o[i]	c
G28.28−0.36	2007-07-11	150 ± 20	49.0 ± 0.3	2.2 ± 0.4	3.0[h]	62.0[c]		c
G30.71−0.06	2007-07-11	88 ± 20	91.5 ± 0.4	4.9 ± 0.8	4.9[h]	87.0[c]		c
G30.82−0.05	2007-07-11	70 ± 20	97.5 ± 0.3	5.1 ± 0.5	4.9[f]	18.0[c]		c
G31.28+0.06	2007-07-19	92 ± 20	109.3 ± 0.3	2.9 ± 0.5	5.8[f]	71.0[c]		c
G31.41+0.31	2007-07-19	100 ± 20	97.4 ± 0.3	3.0 ± 0.4	6.6[f]	11.0[c]		c
G318.95−0.20	2007-07-24	200 ± 20	–34.5 ± 0.3	1.9 ± 0.3	10.6[f]	569.2[d]	o[l],w[j]	c,a,b,d

but not all. The absence of HC_5N detections may also be due to any HC_5N transitions falling below the sensitivity limit. Alternatively, the HC_5N may be emitting from another region outside the hot molecular core but still within the beam, for instance a cold, dense envelope surrounding the hot molecular core. Further, higher sensitivity ATCA observations of HC_5N in these sources along with high-sensitivity observations of a hot core tracer such as CH_3CN may be able to resolve this issue. Spatial comparison of the HC_5N detections with archived MALT90 CH_3CN data was attempted to investigate whether a cold or warm envelope was the source of the HC_5N detections. MALT90, however, is a mapping project and its detections were too weak to offer good spatial comparison for our HC_5N detections, which had significantly longer integration times.

The peak brightness temperature of the molecular lines N_2H^+ (1–0), CH_3CN (5–4 and/or 6–5), thermal CH_3OH (2–1), HCO^+ (1–0), and HNC (1–0) (Purcell et al. 2006, 2009) are compared with the flux of HC_5N detections and non-detections in Fig. 7. Source Sgr B2 has been excluded from this figure for reasons previously discussed along with source G28.85−0.23 which has been excluded due to lack of data for comparison. In addition, sources G10.48+0.03 and

Table 2. Non-detections of HC_5N. These sources fall below the 3σ detection limit of 54 mK. Column 1 is the Source name; Column 2 is the Date of observation; Column 3 is the Kinematic distance; Column 4 is the Methanol peak flux density; Column 5 indicates presence of OH masers with an 'o' and water masers with a 'w' (all sources are methanol masers except the three maserless cores); Column 6 indicates the molecules detected, with 'c' indicating CH_3CN (Purcell et al. 2006), 'a' indicating HC_3N (MALT90 Survey data), 'b' indicating HCN, 'd' indicating HNC (Purcell et al. 2006, 2009. Additional reference is MALT90 data cubes). A† indicates 'maserless' cores (Purcell et al. 2006). References for quoted peak flux densities, distances and masers are: [a]Caswell et al. (2010), [b]Green et al. (2010), [c]Pestalozzi et al. (2005), [d]Green & McClure-Griffiths (2011), [e]Caswell et al. (2011), [f]Green et al. (2012), [i]Caswell (1998), [j]Breen et al. (2010b), [k]Forster & Caswell (1989).

Source name	Observation dates	Distance (kpc)	$S_{\rm PeakMethanol}$ (Jy)	Masers	Other molecules
G00.21−0.00	2006-08-05, 2008-03-29, 2008-04-09, 2008-04-11	–	3.3[a]	w[j]	
G00.32−0.20	2007-07-24	–	62.60[a]	w[j]	c
G00.50+0.19	2006-07-27, 2007-10-01, 2007-12-27, 2008-05-14	–	24.5[a]	o[j],w[j]	d
G00.84+0.19	2006-07-27, 2007-10-01, 2007-12-27	–	6.6[a]		c,d
G01.15−0.12	2006-07-27	–	3.0[a]		c
G02.54+0.20	2006-08-05, 2007-10-01, 2007-12-28	–	29.4[a]	w[j]	
G06.54−0.11	2006-07-10, 2008-03-29, 2008-04-11	13.9[d]	0.6[b]	w[j]	
G06.61−0.08	2007-05-29, 2007-07-24, 2008-05-14	–	23.4[b]	w[j]	
G09.99−0.03	2006-08-05, 2007-05-29, 2007-07-19, 2008-04-11	12.0[d]	67.6[b]	w[j]	c,b,d
G10.44−0.02	2007-06-15, 2007-07-24	11.0[d]	24.3[b]	o[i],w[j]	c
G11.99−0.27	2006-07-27, 2008-03-29, 2008-04-11	11.7[d]	1.9[b]		
G12.03−0.03	2006-07-27, 2008-03-29, 2008-04-11	11.1[d]	96.3[b]		
G12.18−0.12	2007-06-15, 2007-09-05	–	1.9[b]		
G12.21−0.09	2007-06-15, 2007-09-05	–	11.5[b]		
G14.60+0.02	2007-06-16, 2007-12-27	2.8[d]	2.3[b]		c,d
G15.03−0.67	2007-09-11, 2007-12-27	2.3[d]	47.5[b]		c
G15.03−0.71†	2006-07-10, 2007-09-11, 2007-12-27	–	–		
G19.36−0.03	2007-06-16, 2007-09-11, 2007-09-18	2.3[d]	33.8[b]		c
G19.47+0.17	2007-06-16, 2007-09-11, 2007-12-28	–	–		c
G19.49+0.15	2007-06-16, 2007-09-11, 2007-12-28, 2008-02-22, 2008-03-23, 2008-04-09	2.0[d]	6.0[b]		
G19.61−0.13	2007-06-16, 2007-09-11, 2007-12-28	12.1[d]	12.5[b]	o[k]	c
G19.70−0.27	2007-06-16, 2007-12-28	12.6[d]	10.0[b]		
G21.88+0.01	2007-12-28, 2007-07-05, 2007-07-16	–	15.0[c]		
G22.36+0.07	2007-07-05, 2007-07-16, 2007-10-01	4.6[d]	12.0[c]		c
G23.26−0.24	2007-07-05, 2007-07-11, 2007-07-16	–	4.4[c]		
G23.44−0.18	2007-07-05, 2007-07-16	5.9[d]	77.0[c]	o[k],w[k]	c
G23.71−0.20	2007-07-05, 2007-07-16, 2007-07-19	11.0[d]	9.2[c]		
G28.15−0.00	2007-07-05, 2007-07-19, 2007-10-01, 2007-12-28	5.3[d]	34.0[c]	o[i]	c
G28.31−0.39	2007-07-11, 2007-10-01, 2007-12-28	10.4[d]	62.0[c]		
G28.83−0.25	2007-07-11	4.6[d]	73.0[c]		
G28.85−0.23	2007-07-11	5.4[d]	1.9[c]		
G29.87−0.05	2007-07-11	–	67.0[c]		
G29.96−0.02	2007-07-11	9.3[d]	206.0[c]		c
G29.98−0.04	2007-07-11, 2007-12-28, 2008-05-14	9.2[d]	14.0[c]		c
G30.59−0.04	2007-07-11, 2008-03-17, 2008-03-23, 2008-04-09, 2008-05-14	2.7[d]	7.5[c]		
G30.76−0.05	2007-07-11	4.8[d]	68.0[c]		c
G30.78+0.23	2007-07-19	–	19.0[c]		
G30.79+0.21	2007-07-19	9.9[d]	23.0[c]		c
G30.82+0.28	2007-07-11, 2007-07-19	5.6[d]	8.0[c]		c
G30.90+0.16	2007-07-11	5.6[d]	95.2[c]		c
G316.81−0.06	2007-05-29, 2007-06-15, 2007-06-16, 2007-07-24, 2008-03-23, 2008-04-09	2.6[d]	52.0[f]	o[j],w[j]	c,a,b,d
G323.74−0.26	2007-05-29, 2007-06-15, 2007-07-24, 2008-03-23, 2008-04-09	2.8 [d]	3114.4[f]	o[j],w[j]	c,a,b,d
G331.28−0.190	2007-05-29, 2007-06-15, 2007-07-24, 2008-03-23, 2008-03-29, 2008-04-09	4.4[d]	90.0[e]	o[j],w[j]	c,a,b,d
G332.73−0.62	2007-05-29, 2007-06-15, 2007-07-24, 2008-03-23, 2008-03-29, 2008-04-09	3.0[d]	5.1[e]	o[j],w[j]	c,b,d

G318.95−0.20 along with 11 of the non-detection sources have also been excluded from Fig. 7(b) for this reason. Approximately the same range of intensities for the detected molecule is spanned both when HC_5N has, and has not, been detected. However, in the case of N_2H^+, approximately half the detections of this molecule when HC_5N has not been seen fall well below their intensities when HC_5N has been detected. In other words, N_2H^+ is significantly brighter in sources with HC_5N detections than without. HC_5N and N_2H^+ trace cold, dense gas with critical densities[4] of $\sim 10^5$ and $\sim 10^6$ cm^{-3}, respectively. N_2H^+, as well as tracing cold gas, can be found with significant optical depth in warm clouds (Pirogov et al. 2003). Although N_2H^+ was a component of the reaction networks of Chapman et al. (2009), they did not examine or comment on the behaviour of this ion or on relationships with HC_5N. Thus, it cannot be fully determined whether this result is consistent with the modelling of Chapman et al. (2009). Chemical modelling of pre-stellar cores performed by Aikawa et al. (2001), however, found N_2H^+ column density increased with the contraction of the dense molecular cloud core. Aikawa et al. (2001) propose that due to its relatively large depletion time-scale and time-dependent column density, N_2H^+ may

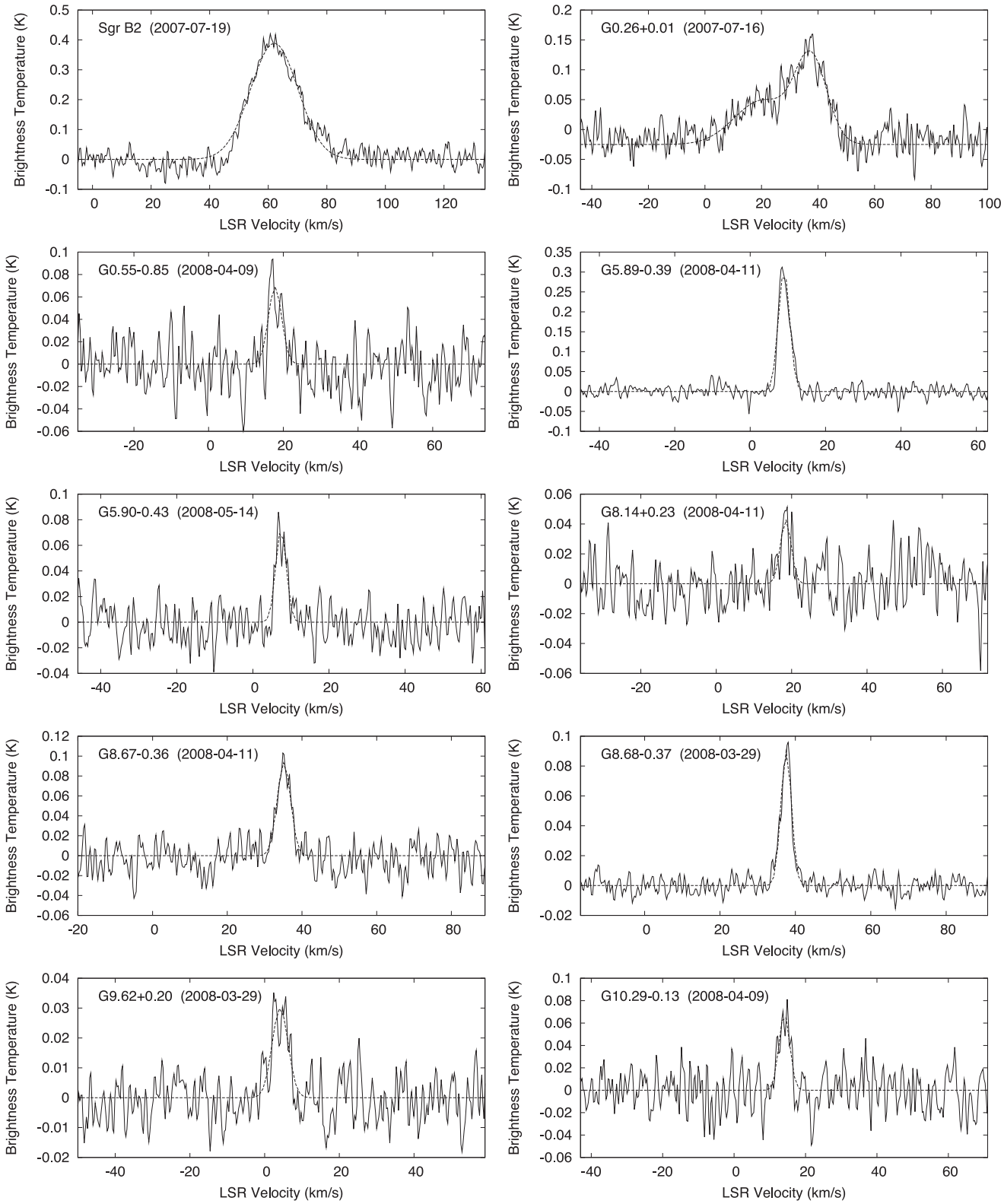

Figure 2. Spectra of the 35 HC_5N detections. Source name and epoch of observation are listed in the top-left corner of each spectra. The dashed line represents the Gaussian fit, as per parameters listed in Table 1.

be a good indicator of core evolution. The increase in N_2H^+ column density during core collapse and its long depletion time-scale may explain the correlation seen in Fig. 7(a) between the peak brightness temperature of HC_5N and N_2H^+, suggesting high levels of N_2H^+ occur in the same evolutionary phase that HC_5N is present. As N_2H^+ will likely outlast the fragile HC_5N, confined to a more limited evolutionary window, it thus may be possible to construct a chemical clock utilizing these species. Peak brightness temperature

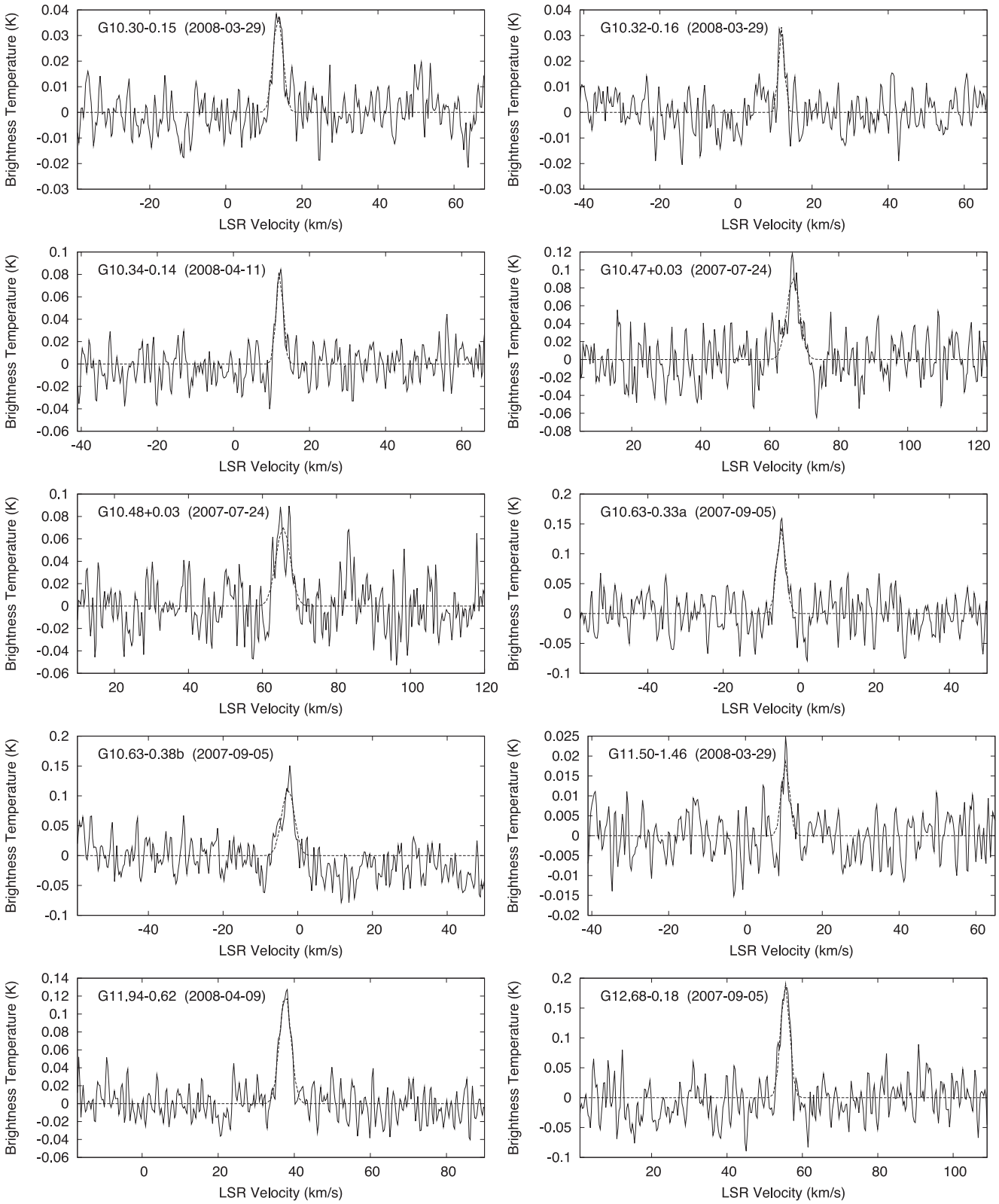

Figure 2 – *continued*

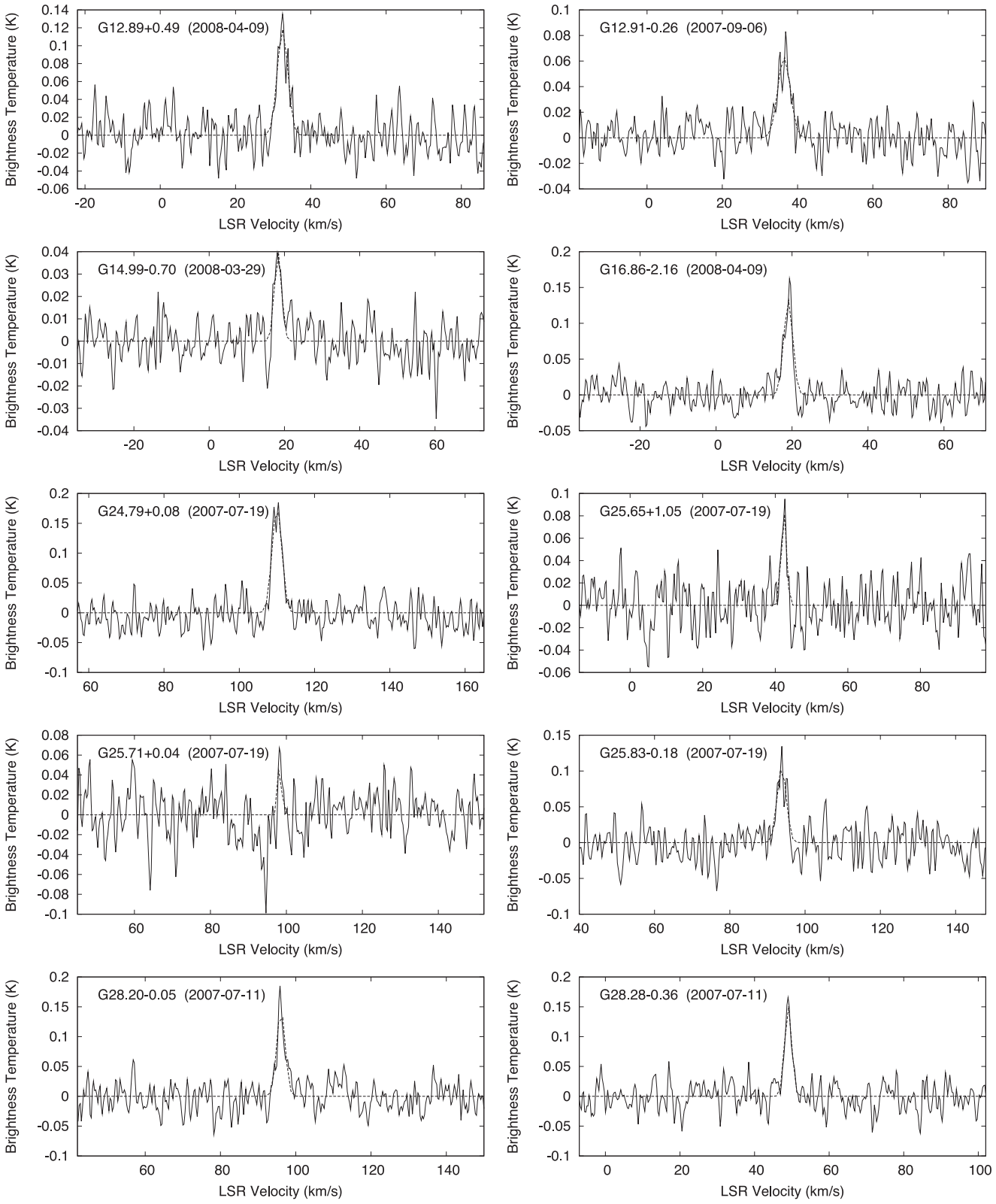

Figure 2 – *continued*

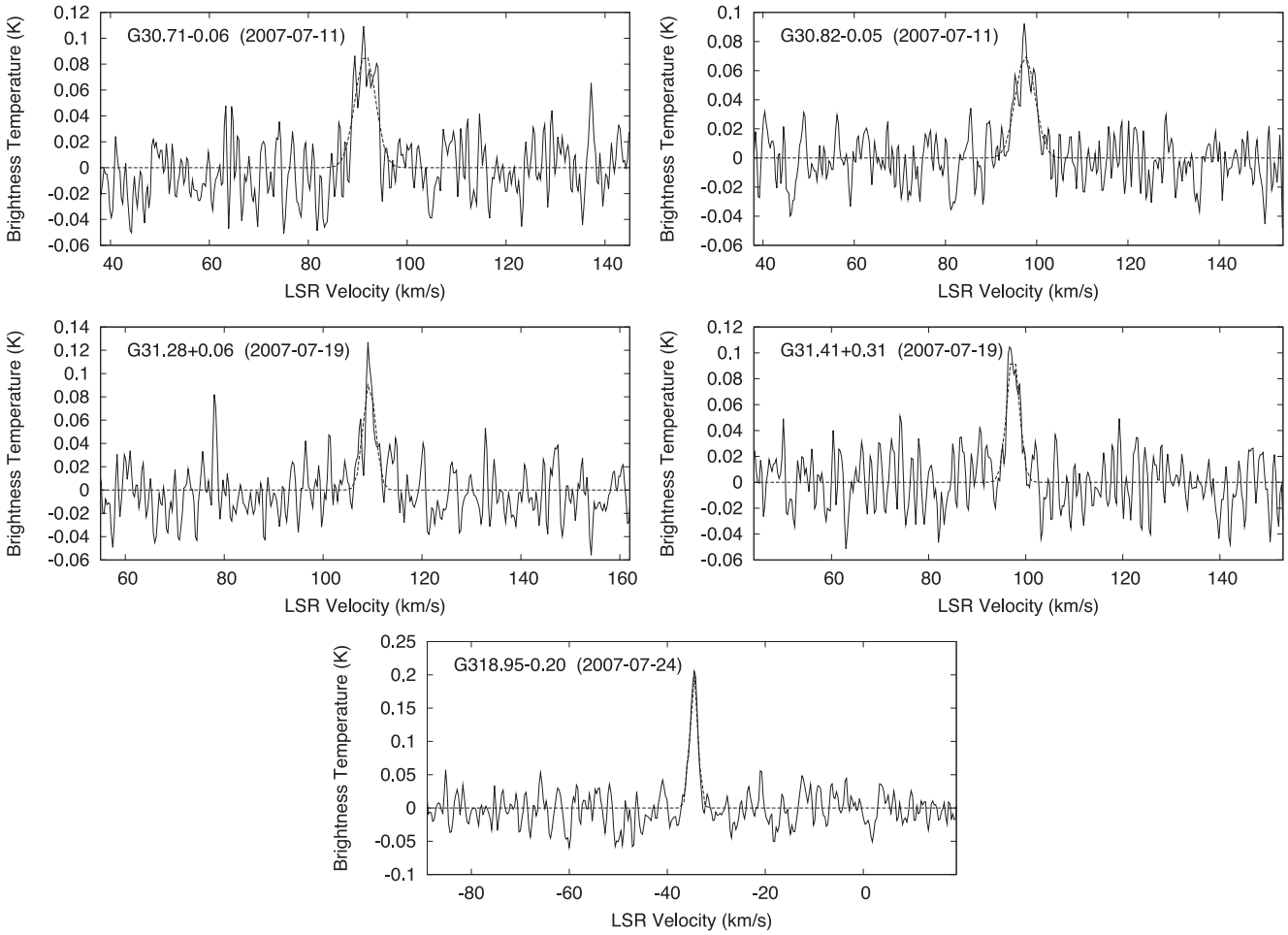

Figure 2 – *continued*

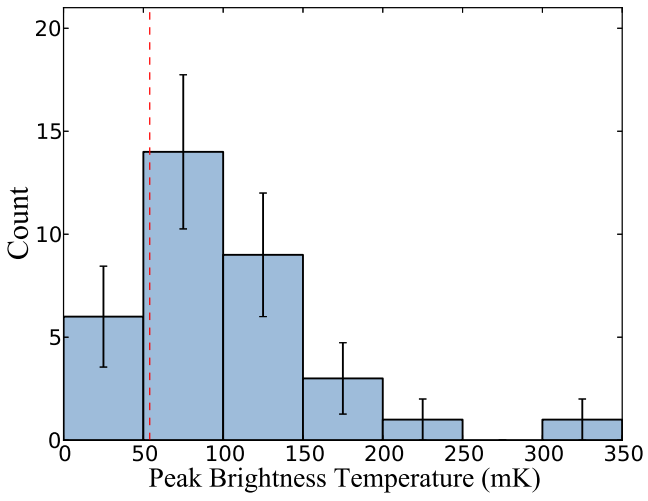

Figure 3. Distribution of peak brightness temperatures. The red dashed line indicates the 3σ sensitivity limit. Error bars represent the statistical (Poisson) error.

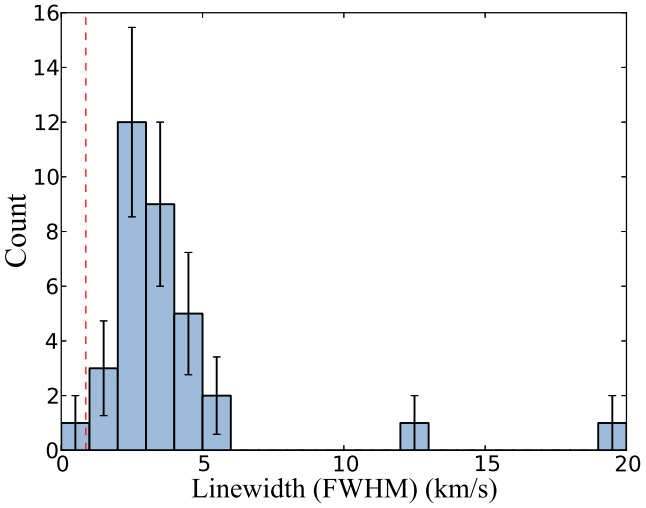

Figure 4. Distribution of linewidths. The red dashed line indicates the width of three channels. Error bars represent the statistical (Poisson) error.

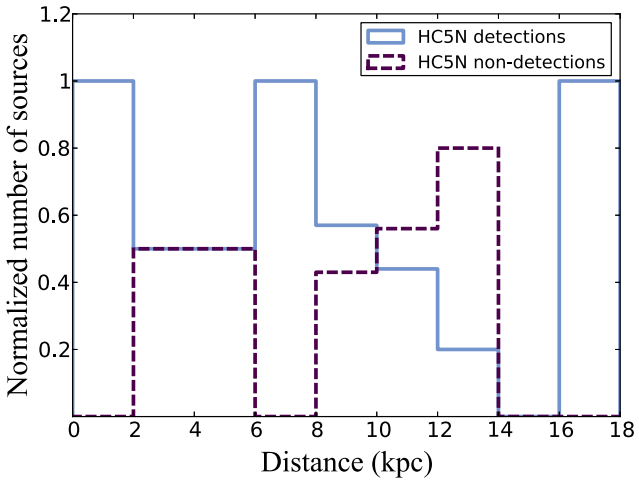

Figure 5. HC_5N detections and kinematic distance. The count per bin has been normalized such that the total number of sources in each bin is one. Distance is not a factor in detection statistics.

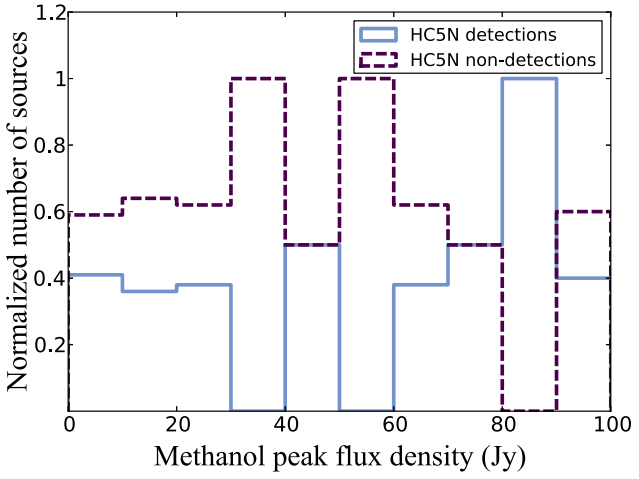

Figure 6. HC_5N detections and methanol peak flux density. The count per bin has been normalized such that the total number of sources in each bin is one. Methanol peak flux density is not a factor in detection statistics.

of HC_5N has also been compared with the 1.2 mm infrared flux (Hill et al. 2005) in Fig. 7(b). Sources with HC_5N detections also appear in general to have greater 1.2 mm infrared flux than those with non-detections.

4.3 Implications for star formation

The results demonstrate that HC_5N may be present in the hot molecular core stage of high-mass star formation, providing support for the Chapman et al. (2009) model. This model indicates that the column densities of HC_5N, HC_7N and HC_9N peak $\sim 1 \times 10^{4.3}$ yr after the onset of core collapse. The abundances fall off rapidly by $\sim 1 \times 10^{5.3}$ yr and then settle to much lower steady state abundances by $\sim 1 \times 10^6$ yr. This suggests that the 35 detections are aged between 1×10^4 and 1×10^6 yr (Breen et al. 2010a). Methanol masers (6.7 GHz) are expected to be present between 1×10^4 and 4.5×10^4 yr, considerably narrowing the age estimate of the detections to within these times. It was also found that of the 35 detections, 13 were associated with OH masers and 20 with water masers. Of the non-detections 9 were associated with OH masers and 13 with water masers. OH masers are expected between $\sim 2 \times 10^4$ and $\sim 4.5 \times 10^4$ yr, while water masers are expected between $\sim 1.5 \times 10^4$ and $\sim 4.5 \times 10^4$ yr (Breen et al. 2010a).

Chapman et al. (2009) propose that the column density ratios of HC_5N and CH_3CN, which increases rapidly between 1×10^4 and $1 \times 10^{5.5}$ yr, may be useful in establishing a chemical clock for the stages of star formation. As we have made detections of both these molecules simultaneously in numerous sources, we have shown this to be a plausible application of HC_5N detections to determine the age of hot molecular cores.

We have compared our observational results to the gas-phase Chapman et al. (2009) chemical model and identify HC_5N as a good candidate to construct a chemical clock. However, hot core chemistry may be a result of a complex combination of gas-phase and grain-surface chemical processes (Garrod & Herbst 2006; Garrod, Weaver & Herbst 2008). Grain-surface chemical models also show HC_5N may exist under the higher temperature conditions of hot cores (Garrod et al. 2008). The choice of model for comparison may, however, introduce some uncertainty in the approximate timeframes of the existence of this molecule and thus into a chemical clock constructed with HC_5N and other molecules such as CH_3CN or N_2H^+. Other uncertainties in such a chemical clock may be introduced by the dependence of the N_2H^+ abundance on that of CO and other species through which this ion can be depleted by proton transfer (Snyder, Watson & Hollis 1977). Despite this, HC_5N remains a good candidate with which to construct a chemical clock to further illuminate the evolutionary age of hot molecular cores and the progress of high-mass star formation.

5 SUMMARY AND CONCLUSIONS

We have made 35 detections of HC_5N, and 44 non-detections towards methanol maser selected hot molecular cores at a 3σ sensitivity limit of 54 mK. Previous modelling by Chapman et al. (2009) shows that HC_5N can form efficiently under the conditions of hot molecular cores and our observations support this. No clear relationships between detections of HC_5N with distance or associated methanol maser peak flux density were found. Sources with HC_5N detections also had detections of CH_3CN. In most HC_5N non-detection sources CH_3CN and N_2H^+ were also present. When HC_5N was detected, however, N_2H^+ was invariably brighter than when it was not detected. The results in general support the chemical modelling of Chapman et al. (2009). However, contrary to preliminary results presented in that work, we find CH_3CN is detected in sources where detections and non-detections of HC_5N have been made.

The study of organic molecules in interstellar clouds is key to finding species which can be used as chemical clocks to help determine the evolutionary age of hot molecular cores and further understand the process of high mass star formation. High resolution observations of the HC_5N $J = 14 \rightarrow 13$ transition with the Atacama Large Millimeter Array (ALMA) in a larger sample of these cores would go far in furthering this research, providing imaging of the gas and their relative locations within the beams we have used in this study (the $J = 12 \rightarrow 11$ transition at 31.95 GHz lies just outside Band 1 of ALMA, while the $J = 14 \rightarrow 13$ at 37.28 GHz lies within it). This would allow verification of whether cold cores lie within the beam, or if a warm envelope surrounds the hot core. Single dish observations of HC_7N and HC_9N would also serve to verify whether long chain cyanopolyynes can exist under hot core conditions and provide a further test of the Chapman et al. (2009) model.

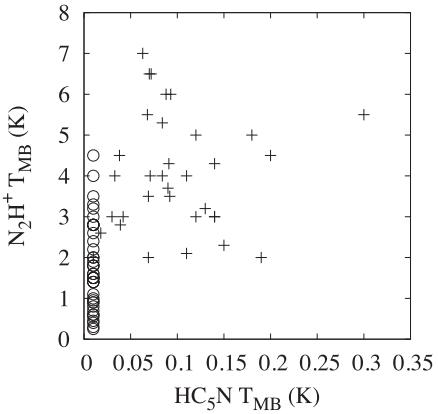

(a) N_2H^+ and HC_5N peak brightness temperature. Sources G0.26+0.01 and G28.20–0.05 overlap at point (0.14, 3).

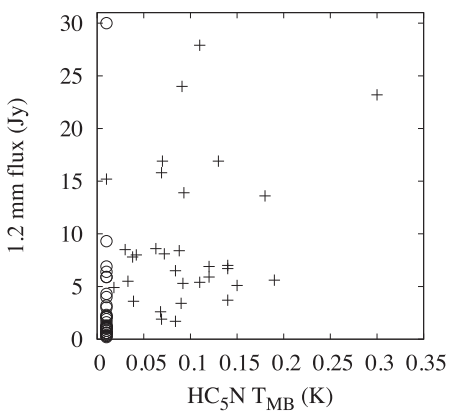

(b) 1.2 mm flux and HC_5N peak brightness temperature

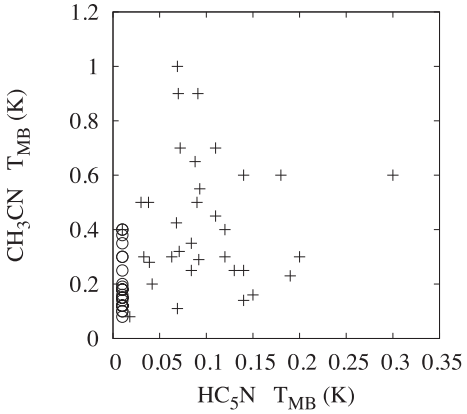

(c) CH_3CN and HC_5N peak brightness temperature.

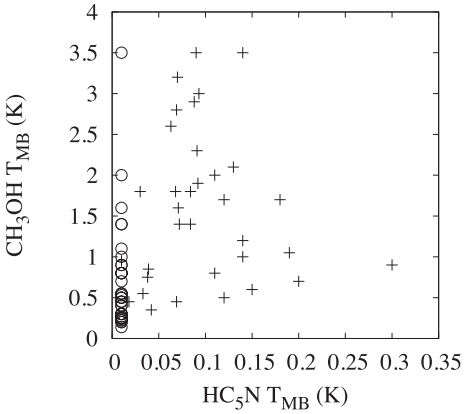

(d) Thermal CH_3OH and HC_5N peak brightness temperature.

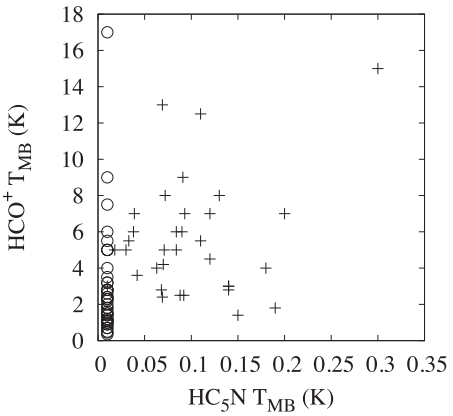

(e) HCO^+ and HC_5N peak brightness temperature. Sources G0.26+0.01 and G10.63–0.38a overlap at point (0.14, 3).

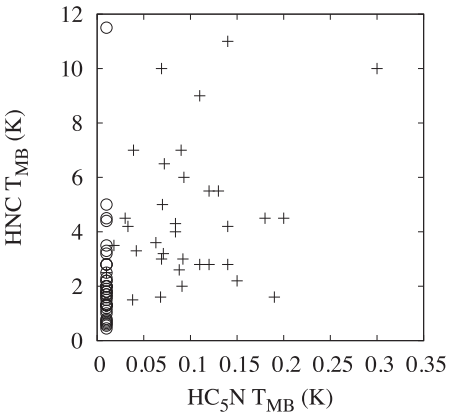

(f) HNC and HC_5N peak brightness temperature.

Figure 7. Molecular comparisons. Peak brightness temperature of corresponding pairs for HC_5N, against N_2H^+, 1.2 mm flux, CH_3CN, Thermal CH_3OH, HCO^+ and HNC. All peak brightness temperatures have been corrected on to the main beam scale. The crosses represent HC_5N detections, the circles represent HC_5N non-detections with main beam peak brightness temperature upper limits of 0.018 K, the 1σ detection limit. Reference for N_2H^+, CH_3CN, Thermal CH_3OH, HCO^+, HNC molecular data is Purcell et al. (2006, 2009). The error margins (1σ) of each of these measurements are, respectively, ∼47 mK, ∼80 mK, ∼76 mK, ∼200 mK and ∼42 mK. Reference for 1.2 mm IR data is Hill et al. (2005). The error margin (1σ) of these measurements is ∼150 mJy. Sources Sgr B2 and G28.85−0.23 have been excluded from this figure.

ACKNOWLEDGEMENTS

We thank the anonymous referee for constructive comments which helped improve the paper. We gratefully acknowledge the use of MALT90 Survey spectral line data cubes in the course of this project. We also acknowledge Australian Research Council (ARC) support through Discovery Project DP0451893 awarded to The University of New South Wales and Macquarie University. Astrophysics at Queens University Belfast is supported by a grant from the Science and Technology Facilities Council (STFC). The Tidbinbilla 34 m DSS–34 Radio Telescope is part of the Canberra Deep Space Communication Complex, which is operated by CSIRO Astronomy and Space Science on behalf of NASA.

REFERENCES

Aikawa Y., Ohashi N., Inutsuka S.-I., Herbst E., Takakuwa S., 2001, ApJ, 552, 639
Aikawa Y., Wakelam V., Garrod R. T., Herbst E., 2008, ApJ, 674, 984
Aikawa Y., Wakelam V., Hersant F., Garrod R. T., Herbst E., 2012, ApJ, 760, 40
Avery L. W., Oka T., Broten N. W., MacLeod J. M., 1979, ApJ, 231, 48
Breen S. L., Ellingsen S. P., Caswell J. L., Lewis B. E., 2010a, MNRAS, 401, 2219
Breen S. L., Caswell J. L., Ellingsen S. P., Phillips C. J., 2010b, MNRAS, 406, 1487
Breen S. L., Ellingsen S. P., Contreras Y., Green J. A., Caswell J. L., Stevens J. B., Dawson J. R., Voronkov M. A., 2013, MNRAS, 435, 524
Broten N. W., MacLeod J. M., Oka T., Avery L. W., Brooks J. W., McGee R. X., Newton L. M., 1976, ApJ, 209, L143
Caswell J. L., 1998, MNRAS, 297, 215
Caswell J. L., 2009, Publ. Astron. Soc. Aust., 26, 454
Caswell J. L. et al., 2010, MNRAS, 404, 1029
Caswell J. L. et al., 2011, MNRAS, 417, 1964
Chapman J. F., Millar T. J., Wardle M., Burton M. G., Walsh A. J., 2009, MNRAS, 394, 221
Forster J. R., Caswell J. L., 1989, A&A, 213, 339
Fukuzawa K., Osamura Y., Schaefer H. F., III, 1998, ApJ, 505, 278
Garrod R. T., Herbst E., 2006, A&A, 457, 927
Garrod R. T., Weaver S. L. W., Herbst E., 2008, ApJ, 682, 283
Goddi C., Greenhill L. J., Humphreys E. M. L., Matthews L. D., Tan J. C., Chandler C. J., 2009, ApJ, 691, 1254
Green J. A., McClure-Griffiths N. M., 2011, MNRAS, 417, 2500
Green J. A. et al., 2010, MNRAS, 409, 913
Green J. A. et al., 2012, MNRAS, 420, 3108
Hill T., Burton M. G., Minier V., Thompson M. A., Walsh A. J., Hunt-Cunningham M. R., Garay G., 2005, MNRAS, 363, 405
Hirota T., Yamamoto S., 2006, ApJ, 646, 258
McMillan P. J., Binney J. J., 2010, MNRAS, 402, 934
Millar T. J., Macdonald G. H., Gibb A. G., 1997, A&A, 325, 1163
Minier V., Ellingsen S. P., Norris R. P., Booth R. S., 2003, A&A, 403, 1095
Müller H. S. P., Thorwirth S., Roth D. A., Winnewisser G., 2001, A&A, 370, L49
Müller H. S. P., Schlöder F., Stutzki J., Winnewisser G., 2005, J. Mol. Struct., 742, 215
Olmi L., Cesaroni R., Walmsley C. M., 1993, A&A, 276, 489
Pestalozzi M. R., Minier V., Booth R. S., 2005, A&A, 432, 737
Pirogov L., Zinchenko I., Caselli P., Johansson L. E. B., Myers P. C., 2003, A&A, 405, 639
Purcell C. R. et al., 2006, MNRAS, 367, 553
Purcell C. R., Longmore S. N., Burton M. G., Walsh A. J., Minier V., Cunningham M. R., Balasubramanyam R., 2009, MNRAS, 394, 323
Rathborne J. M., Lada C. J., Muench A. A., Alves J. F., Lombardi M., 2008, ApJS, 174, 396
Reid M. J., Menten K. M., Zheng X. W., Brunthaler A., Xu Y., 2009, ApJ, 705, 1548
Sakai N., Sakai T., Hirota T., Yamamoto S., 2008, ApJ, 672, 371
Sakai N., Sakai T., Hirota T., Burton M., Yamamoto S., 2009, ApJ, 697, 769
Schönrich R., Binney J., Dehnen W., 2010, MNRAS, 403, 1829
Seki K., Yagi M., Maoqi H., Halpern J. B., Okabe H., 1996, Chem. Phys. Lett., 258, 657
Snyder L. E., Watson W. D., Hollis J. M., 1977, ApJ, 212, 79
Stahler S. W., 1984, ApJ, 281, 209
Turner B., 1991, ApJS, 76, 617
Walsh A. J., Hyland A. R., Robinson G., Burton M. G., 1997, MNRAS, 291, 261
Walsh A. J., Burton M. G., Hyland A. R., Robinson G., 1998, MNRAS, 301, 640
Walsh A. J., Macdonald G. H., Alvey N. D. S., Burton M. G., Lee J.-K., 2003, A&A, 410, 597
Wyrowski F., Schilke P., Walmsley C. M., 1999, A&A, 341, 882

This paper has been typeset from a TEX/LATEX file prepared by the author.